HHS Public Access

Author manuscript

Science. Author manuscript; available in PMC 2023 February 18.

Published in final edited form as:

Science. 2022 February 18; 375(6582): 745–752. doi:10.1126/science.abn1395.

Modular terpene synthesis enabled by mild electrochemical couplings

Stephen J. Harwood[1,†], **Maximilian D. Palkowitz**[1,†], **Cara N. Gannett**[2], **Paulo Perez**[3], **Zhen Yao**[4], **Lijie Sun**[4], **Hector D. Abruña**[2,*], **Scott L. Anderson**[3,*], **Phil S. Baran**[1,*]

[1]Department of Chemistry, Scripps Research, La Jolla, CA, 92037, USA.

[2]Department of Chemistry and Chemical Biology, Baker Laboratory, Cornell University, Ithaca, NY, 14853, USA

[3]Department of Chemistry, University of Utah, 315 S. 1400 E., Salt Lake City, UT, 84112, USA

[4]Asymchem Life Sciences (Tianjin) Co., Ltd. No. 71, 7th Ave., TEDA Tianjin, 300457, P.R. China

Abstract

The synthesis of terpenes is a large field of research that is woven deeply into the history of chemistry. Terpene biosynthesis is a case-study of how the logic of a modular design can lead to diverse structures with unparalleled efficiency. This work mimics Nature by leveraging modern Ni-catalyzed electrochemical sp^2–sp^3 decarboxylative coupling reactions—enabled by Ag-nanoparticle modified electrodes—to intuitively assemble terpene natural products and complex polyenes using simple modular building blocks. The step-change in efficiency of this approach is exemplified through the scalable preparation of 13 complex terpenes, which minimized protecting group manipulations, functional group interconversions, and redox fluctuations. The mechanistic aspects of the essential functionalized electrodes are studied in depth through a variety of spectroscopic and analytical techniques.

One Sentence Summary:

A scalable platform reliant on Ag-nanoparticle functionalized electrode and Ni-catalysis enables practitioners to mimic the way Nature modularly assembles terpenes.

The study of terpene synthesis holds a special place in the annals of organic synthesis, with the formalization of the stereoelectronic effect, conformational analysis, rules for pericyclic reactions, and even retrosynthetic analysis stemming from this field.(1) Beyond synthesis,

*Correspondence to: hda1@cornell.edu, anderson@chem.utah.edu, pbaran@scripps.edu.
†These authors contributed equally to this work.

Author Contributions: S.J.H. and P.S.B. conceived of the work. S.J.H., M.D.P., C.N.G, P.P., H.D.A., S.L.A., and P.S.B. designed the experiments. S.J.H., M.D.P, C.N.G., P.P, ran the experiments. S.J.H, M.D.P, C.N.G, P.P., H.D.A., S.L.A. and P.S.B. analyzed the data. Z.Y. and L.S. conducted the flow-reactor scale up. S.J.H., M.D.P. and P.S.B wrote the manuscript. C.N.G., P.P., H.D.A. and S.L.A. provided revisions.

Competing interests: The authors declare no competing interests.

Data and Materials Availability: Experimental and analytical procedures and full spectral data are available in the supplementary materials. X-ray data and models are available at the Cambridge Crystallographic Data Centre under accession numbers CCDC-2033224 (**S12**) and CCDC-2109535 ($NiCl_3(PtBu_3)$ • $HPtBu_3$).

the pivotal role that terpenes play in nature and medicine has inspired practitioners from a wide spectrum of the scientific community.(2, 3) As medicines, they exhibit broad activity ranging from modulation of human physiology (e.g., steroid hormones, cannabinoids) to amelioration of disease (e.g., Taxol®, artemisinin).(2) Terpenes also pervade the fine chemicals industry and are found in commercial fragrances and food additives.(4) Not surprisingly, this class of natural isolates has inspired numerous total syntheses, a legendary example being Johnson's synthesis of progesterone in 1971 (Figure 1A).(5) As one of the first biomimetic terpene syntheses, it validated the Stork-Eschenmoser hypothesis by stitching together the polycyclic steroid core through a bold cation-olefin cyclization.(6) This tactic subsequently shaped the landscape of future chemical approaches to such molecules through its ability to generate polycyclic ring-systems and multiple stereocenters from prochiral alkenes. Polyene cyclization is still an active area of research in the modern era, as evidenced by the steady development of new polycyclization reactions and enantioselective variants.(7) Although the power of cation-olefin cyclization is undisputed, the construction of polyunsaturated precursors remains oddly challenging. Retrosynthetic strategies to forge such entities are still plagued with a non-intuitive logic where building blocks used do not clearly map onto the product into which they are ultimately incorporated. Specifically, these approaches are non-modular and individually target each polyolefin cyclization precursor synthesized. Furthermore, they often lack complete control of olefin geometry (a critical feature controlling the resulting sp^3 stereochemistry), and require multiple functional group interconversions (FGIs).(8) The current barrier to rapid, modular, and controlled polyene construction therefore limits the effectiveness of what is arguably one of the most powerful complexity-inducing chemical transformations known. Meanwhile, steady advancement in the development of methodology for creating sp^2–sp^3 linkages has pointed towards a simpler approach to polyene synthesis (Figure 1B).(9, 10) The cyclase phase of natural terpene assembly points to inherent advantages of a modular approach as a simple building block like isopentenyl pyrophosphate (IPP) can be intuitively mapped onto the final polyene product.(11) The goal of this study was to mimic this strategy for modular terpene synthesis by focusing on disconnecting sp^2–sp^3 bonds directly to arrive at simple carboxylic acid precursors (Figure 1C). By combining the learnings of decarboxylative C—C bond formation and electrochemical cross-electrophile coupling with a new application of *in situ* electrode functionalization we show how halo-acid modules can be iteratively coupled resulting in more logical retrosynthetic analyses that reduce step-counts and reliance on pyrophoric reagents while removing non-ideal manipulations.(12, 13) The scalable access to 13 terpene natural products exemplifies the strategic power of this logic. Furthermore, the mechanistic interplay between the Ag-embedded heterogeneous interface and the homogenous Ni-catalyst exemplifies the untapped potential of functionalized electrodes in synthetic organic electrochemistry.

[Rationale]

The execution of the plan outlined above would require a departure from many of the (alkenyl)-sp^2–sp^3 disconnection strategies previously used that combine alkyl organometallic reagents or boronates with vinyl halides (Figure 1B).(9, 10) The functional group compatibility needed (tolerating free carboxylic acids, for example) and a desire to

minimize functional group interconversions (e.g. R–X to R–BR_2) was vividly illustrated in our initial forays (Figure 2). Here we enlisted the recently disclosed decarboxylative alkenylation with organozincs (prepared through lithium halogen exchange).(14) In the coupling with redox-active ester (RAE) **2**, more than three equivalents of **1** and six equivalents of *t*-BuLi under cryogenic conditions were required to generate the organometallic. Deprotection and oxidation of the resulting product **3** set the stage for the ensuing coupling. Although conceptually attractive, this approach fell short of the modular and mild aspirations of the initial plan (see SM for discussion). The seminal work of Périchon and Nédélec on electrochemical reductive cross-coupling was inspirational as it demonstrated the coupling of vinyl halides with electronically biased alkyl halides in a simple undivided cell.(15) Additionally, reports adapting this reactivity to aryl-alkyl cross-coupling using alkyl RAEs as alternatives to alkyl halides have emerged.(16) Inspired by these precedents, initial conditions were developed that enabled a more functional group tolerant reductive coupling of pre-generated RAEs with vinyl iodides. Unfortunately, after initial optimization efforts (see SM Tables S31-36) the use of free acid **5** in this milder coupling only provided trace quantities of **6** using an *in situ* protocol for the conversion of **4** to the corresponding RAE. An extensive series of optimization experiments were performed in hope of overcoming this apparently intractable problem. Many of the traditional experimental variables associated with the optimization of electrochemical reactions such as electrolyte and electrode were re-evaluated to no avail. Modification of the properties of the Ni-based electrocatalytic system were also re-explored by screening ligands, Ni-sources, and other metals known to promote reductive coupling. Finally, given the heterogeneous nature of electrochemistry, efforts to modify the surface of the electrode were pursued since the deposition of metals onto electrode materials has been used to improve the performance of reductive electrochemical transformations.(17) Two metals that are known to readily and reproducibly plate onto carbon electrodes, Cu and Ag, were explored with the latter providing a stunning increase in reaction efficiency and functional group compatibility.(18) Thus, addition of 0.30 equiv. $AgNO_3$ relative to the redox active ester starting material to the standard reductive coupling conditions [$NiCl^2$•$6H_2O$ (10 mol%), 2,2’-bpy (10 mol%), DMF, room temperature (r.t.)] resulted in 50% isolated yield of **6**. The precise nature of this electrode modification was studied in detail (*vide infra*) and supported the notion that Ag-based nanoparticles were present and responsible, at least in part, for this enhanced outcome. Before applying these newly developed conditions, a number of control studies were undertaken as illustrated at the bottom of Figure 2. Using coupling partners **5** and **7** as model substrates that give measurable yields without $AgNO_3$, several experiments confirmed that the Ag ion was the essential additive (entries 1-3). Entries 4-6 corroborate the role of Ag-based nanoparticles as the use of pure Ag electrodes or Ag-plated electrodes did not work well whereas Ag-nanoparticles, deposited on RVC electrodes, could be recycled without the need for added Ag. Finally, the critical role of electrochemistry in this process was confirmed (entries 7-10) by running the reaction in the absence of current or by employing stoichiometric chemical (Mg) reductants, although, addition of Ag to those non-electrochemical processes did lead to notable improvements. Importantly, previously developed C(sp^3)-C(sp^2) decarboxylative cross coupling conditions were unamenable to the desired decarboxylative alkenylation employing electrophiles such as **7** (See SM, Table S44) (19-21) In the final optimized manifestation, a free carboxylic acid (1.0 equiv.) could be

converted to the NHPI-RAE (N,N'-diisopropylcarbodiimide, N-hydroxyphthalimide, 1-3 h) in a minimal amount of THF (max. 1 mmol/0.75 mL of THF) followed by direct addition of vinyl iodide (1.5 equiv.) and Ni catalyst in DMF (0.07-0.25M); the solution was then added to a commercial electrochemical cell fitted with a sacrificial Mg-anode and RVC-cathode containing $AgNO_3$ (0.3 equiv.). Then, the reaction was electrolyzed (ca. 2.5 F/mol, 2.5 h) at ambient temperature.

[Results]

With a viable method in hand for chemoselective and modular C–C coupling, execution of the blueprint outlined in Figure 1 could be explored. Rather than pursue a tabular listing of coupling partners to illustrate functional group tolerance and geometric control (all stereoretentive), the value of the methodology was exemplified through the total or formal synthesis of 13 terpene natural products (Figure 3). A range of functional groups is tolerated, including epoxides, alkynes, alcohols, free carboxylic acids on the vinyl iodide, esters, ethers, ketones, enones, aldehydes, electron-rich (hetero)aromatics, β-keto esters, and skipped dienes. The simplification enabled by this method is apparent in three polyene cyclization precursors prepared *en route* to complex terpene natural products: progesterone (8), celastrol (9), and isosteviol (10). A protecting group free synthesis of progesterone precursor **8** begins with the electrochemical cross-coupling of two simple acids **4** (*in situ* activated) and **5** (prepared in two steps via carboiodination and oxidation). The product acid **6** was next *in situ* activated and coupled to a vinyl iodide bearing a free alcohol (11). Alcohol **12** was converted to the bromide (13) via Appel conditions and coupled to 2-iodo-3-methylcyclopentenone using an electrochemical reaction inspired by Hansen's electrochemical conditions (See SM Tables S3-6) to deliver the desired polyene endpoint (8) directly.(22) In contrast, similar reported couplings have employed Suzuki conditions which required three steps to prepare a suitable trifluoroborate-containing coupling partner.(23) This modular and intuitive approach takes place in six steps (longest linear sequence, LLS) relying on a single FGI and oxidation step without resorting to any protecting groups. In contrast, Johnson's synthesis of progesterone arrived at the target polyene in 8 steps (LLS) with two FGI's and two PG-related steps.(5) In 2016, Dudley and coworkers published a 10-step total synthesis of progesterone which also prepares polyene **8** in six steps LLS with one FGI and one oxidation.(23)

Siegel's elegant approach to **9** leveraged a unique polyene cyclization precursor bearing a tetra-substituted alkene and an electron rich arene.(24) Cleverly, inherent symmetry was exploited to arrive at the polyene in 9 steps, using one FGI and one oxidation. The use of an HWE reaction led to a 6:1 mixture of *E/Z* isomers, highlighting the challenges associated with approaches that construct polyolefin cyclization precursors through Wittig-like transforms. In contrast, the modular assembly approach breaks bonds adjacent to the olefins and programs the alkene geometry at the outset. The synthesis commences with *in situ* activation of acid **14** and electrochemical coupling with the same vinyl iodide **5** used in the synthesis of **8**. The product acid **15** was subsequently activated and coupled with tetra-substituted vinyl iodide **16** bearing a reactive aldehyde to complete the formal synthesis endpoint of celastrol (9) in 5 steps.

Snider's impressive synthesis of isosteviol relied on pioneering oxidative radical cascade methodology from polyene **10**—prepared in 10-steps (LLS) with 2 FGI's and 3 redox manipulations.(25) Our initial attempts using more traditional organometallic cross-coupling chemistry (Figure 2) yielded no success in the first coupling (see SM, Figure S9). Using vinyl organolithium reagents led to a retro-lithium ene reaction to expel allyl lithium, and treating the allyl vinyl iodide **17** with organometallic reagents led to recovery of vinyl iodide. The only conditions identified capable of forging the desired bond between the acid **18** and skipped diene **17** were the developed electrochemical conditions, which gratifyingly gave the desired product acid **19** in 53% isolated yield on gram-scale. The resulting acid **19** was activated and coupled to vinyl iodide **20** bearing the reactive β-ketoester functionality (a testament to the functional group compatibility of the developed conditions) providing more than a gram of polyene **10** in 6 steps LLS.

To further test the capabilities of the developed methodology, a broad range of terpenes was targeted. The diterpene, ambliol A, first isolated from the marine sponge *Dysidea amblia* by Faulkner in 1981 off of the Pacific coast (La Jolla) was chosen as an attractive target to synthesize for its antibiotic activity and unique functionality.(26, 27) Only recently (2015) was an enantioselective synthesis of (+)-ambliol A accomplished by Serra and Lissoni using an enzymatic resolution in 16 steps LLS.(28) That synthesis led to a revision of the original enantiomeric assignment. In contrast, a convergent synthesis of (–)-ambliol A utilizing the developed electrochemical conditions was achieved in just five steps LLS by coupling the enantiopure epoxyacid **21** (confirmed via x-ray crystallography: See SM, Figure S112) with furan **22** in 47% yield followed by reductive epoxide opening ($LiEt_3BH$) thus unambiguously confirming its stereochemical revision and enabling the first synthetic access to the natural enantiomer.

The sesquiterpenes (*E*)-α- and β-bisabolenes (**23** and **24**), which function in nature as pheromone molecules for a number of insects, were an opportunity to test the electrochemical cross-coupling on secondary acids.(29) Targeting the central sp^2–sp^3 junction for disconnection, syntheses of **23** and **24** diverged from secondary acid **25** and enlisted vinyl iodide **26** or **27** to furnish **23** and **24** in 72% and 64% yield, respectively. The more stabilized secondary radical generated from the acid coupled efficiently under the standard reaction conditions providing access to both natural products in three steps LLS.

The California red scale sex pheromone, produced by an invasive citrus pest, was originally identified in 1977 by Gieselmann and co-workers and is used by the females to attract males.(30) Its synthesis has applications in the agricultural industry as a replacement for virgin female traps in monitoring the pest's population. Strategically, a synthesis was envisioned that leveraged a β-iodo-enoate as a lynchpin fragment capable of forging 3 key C—C bonds off the central two carbon linker. This concept was realized by first cross-coupling 4-pentenoic acid with methyl (*E*)-3-iodoacrylate in 54% yield, followed by a conjugate addition and saponification in 80% and 86% respectively to provide acid **28**. The synthesis could be completed by coupling **28** and acetate **29**; however, upon generation of the primary radical under the reaction conditions, it underwent a 5-exo-trig cyclization before cross-coupling of the vinyl iodide could take place. This problem was obviated by

increasing the nickel catalyst loading to 40 mol% to provide California red scale pheromone in 56% yield and six steps LLS.(31)

The importance of the homologated terpene (*E,E*)-homofarnesol (30) stems from its use as a cyclization precursor to the vital terpene Ambrox ® (ambroxide)—a molecule with a storied history dating back to the 15th century.(32) Many of the reported syntheses of **30** rely on [2,3] rearrangements of the nerolidols that lead to mixtures of *E/Z* isomers which, if not carefully separated, give complex mixtures of cyclization products that harm its fragrant properties.(33) In contrast, acid **31** (readily prepared from geranyl bromide and diethyl malonate) was *in situ* activated and coupled with vinyl iodide **32** bearing a free alcohol to arrive directly at (*E,*E)-homofarnesol (>4 grams prepared in single pass).

The diterpene geranyl linalool was synthesized through two sequential cross-couplings of common fragments: one of which was employed in the synthesis of progesterone and celastrol and the other two of which were used to access nerolidols (Figure 3B). This mix-and-match strategy for opportunistically accessing naturally occurring terpenes highlights the advantage of using the modular logic also employed in the biosynthetic cyclase phase.

Notwithstanding the value of the disclosed methods to the academic pursuit of complex terpene total synthesis, nowhere is the study and utilization of linear terpenes more apparent than in the fragrance and flavor industry (>$30-billion-dollar *per annum*).(4) Given the sensitivity of human olfactory receptors, single terpene isomers of high purity are desired to ensure precise flavor and fragrance profiles because small changes in structure can create very different properties.(34, 35) One class of terpene targets, nerolidol, seemed particularly relevant in this context. A unified, controllable synthesis of the linear terpenes (*E*)- and (*Z*)-nerolidol, produced naturally as a mixture of four isomers derived from nerol and geraniol, has remained an unanswered synthetic challenge for over four decades. Whereas their synthesis and separation have been explored, preparative methods of separation or synthesis are expensive and laborious.(36) Indeed, the extreme price disparity between the racemic mixture of isomers (ca. $0.09/gram Sigma-Aldrich), and the geometrically pure racemate (*trans:* $610/g, Sigma-Aldrich; *cis*: $343-2460/gram, various suppliers) is cost-prohibitive and the enantiopure natural products are not commercially available. Despite the difficulty in purification, nerolidol is estimated to be used *per annum* in quantities between 10 to 100 metric tons and appears in products like shampoos, perfumes, detergents and as a flavor additive.(37) The need for a selective and programmable synthesis of these four isomers stems from their differing fragrance profiles.

To synthesize *(E)*- and (*Z*)- nerolidols, we imagined these isomers could arise from two geometrically differentiated vinyl iodides (***E*-33** and ***Z*-33**, respectively) and enantiomeric RAEs derived from (*R*)- and (*S*)-linalool, respectively (***R*-34, *S*-34**). A simple mix-and-match union of the modules resulted in the controlled synthesis of **35–38** in 44%-60% yield after deprotection. As a proof-of-concept for the scalability of the method, **35** was arbitrarily chosen and the electrochemical coupling was performed on 100g scale (at Asymchem, see inset photos). Of note, analysis of the electrodes in this large-scale flow run confirmed that Ag-nanoparticles were present at a surface coverage of Ag analogous to small scale reactions requiring only 0.07 equiv. of Ag (see SM, Figures S47-48).

[Mechanistic Studies]

Although the observations from the above syntheses suggested that the homogenous Ni-catalysis behaved according to literature precedent for radical cross-coupling(31), the impact of electrode surface functionalization on this methodology warranted further study as existing $C(sp^3)$-$C(sp^2)$ decarboxylative coupling conditions failed to match the efficiency of the developed protocol (Figure 4 and SM Table S44). An induction period was observed that corresponded in duration to the amount of $AgNO_3$ added, suggesting that silver reduction preceded the cross-coupling reaction (see SM, Figure S19-20). Despite the use of nanoparticulate silver in heterogenous catalysis, we have not found prior examples in which it supports and/or improves homogenous catalysis in organic synthesis.(38) In contrast, the field of electroanalytical sensors routinely uses electrode functionalization to engender selectivity for a specific analyte, even in the presence of species with nearly identical reduction potentials on unmodified electrode surfaces.(39, 40) This selectivity arises from to the ability of the Ag-nanoparticles to lower the overpotential(41) required to reduce or oxidize an analyte of interest.(42) Additionally, selectivity can manifest as a change in the reduction potential (potential shift to less driving potentials of the voltametric wave) through metal particle-analyte interactions.(43-47) Many analyte-specific sensors have been developed using Ag-nanoparticle decorated electrodes.(43-46) Preparations of Ag modified electrodes for sensor applications include drop casting a suspension of pre-formed Ag-nanoparticles onto a surface and drying, or cathodic reduction of a solution of silver(I), with the latter being strikingly similar to the procedure used in this developed cross coupling reaction.(48) To better understand the interplay between the electrode surface modification by silver and homogenous nickel catalysis, several experiments were conducted.

First, modified electrode surfaces were characterized using Scanning Electron Microscopy (SEM) imaging, Transmission Electron Microscopy (TEM) and Energy-Dispersive x-ray Spectroscopy (EDS)(Figure 4B). When $AgNO_3$ alone was electrodeposited prior to the start of the reaction, the glassy carbon electrodes were coated with a gray film. The use of these modified electrodes yielded only 24% of product **39** between RAE **7** and vinyl iodide **5**. SEM imaging showed that while large silver crystals formed (1-5 μm in diameter), there were very low levels of nanoparticulate silver on the electrode surface. However, addition of LiCl to this pre-reaction electrodeposition produced electrodes with improved reaction performance (41% NMR yield). SEM and TEM analyses of these electrode surfaces revealed the presence of nanoparticulate silver in sizes ranging 10 to 100 nm in diameter (See SM, Figures S36-40). Controls verified the need for a halide source but LiCl was not required in the coupling reactions since $NiCl_2$ could serve as the halide donor in the preparative reactions. The reaction of $AgNO_3$ and halides in solution produces photosensitive silver halide salts that readily decompose. Electrodes modified using a $AgNO_3$ and LiCl solution that had been allowed to stir for several minutes before electrolysis were evaluated in the coupling reaction. In such cases, only a 17% yield of **39** was obtained and very little nanoparticulate silver was observed in microscopic characterization (See SM, Figure S44-45). Collectively, these results suggest that nanoparticulate silver electrodeposited before the cross-coupling reaction is present and responsible, at least in part, for the improved performance.

Seeking to compare reactivity of these nanoparticle-coated electrodes in the cross-coupling with known reactivity of similarly functionalized electrodes, glassy carbon disk electrodes were also functionalized. Nanoparticle deposition on this disk electrode was validated by anodic stripping voltammetry (Figure 4B) and S/TEM imaging (See SM, Figure S50-51).(43) The reduction potential of benzyl chloride is known to shift 500 mV more positive on a silver-nanoparticle decorated electrode and such behavior was observed on our nanoparticle-coated disk.(46) Cyclic voltametric studies of reductively labile components of the cross coupling, $NiCl_2$(bpy) and RAE **7**, revealed no significant differences in the onset of reduction of these two species at the functionalized electrode in comparison to glassy carbon surfaces (See SM, Figures S54-76).

The kinetic behavior of the modified electrode was then studied using rotating disk electrode (RDE) voltammetry.(49) In the case of $NiCl_2$(bpy), a diminished current response in consecutive cycles at an unmodified glassy carbon RDE was observed. The decrease in the current with cycling is mitigated if the potential range is limited to a smaller (less negative) reductive window (lower potential cutoff of −1.6 V vs. Ag/AgCl, Figure S83). Additionally, when the same measurements were performed with the silver-nanoparticle modified RDE, the peak current response of the Ni(II)/Ni(0) redox couple was slightly lower and its current also decreased with continuous cycling, but at a notably slower rate (Figure 4C-I). The initial current response could be restored to the glassy carbon electrode by a potential excursion to +1.5 V vs. Ag/AgCl, indicating that passivation is likely occurring through over-reduction and deposition of the catalyst on the electrode surface. Supporting this hypothesis, the cathode potential (at constant current) of the reaction revealed a significant difference between the reactions with and without $AgNO_3$. The potential of the reaction in the presence of $AgNO_3$ ($E_{cathode}$ = −1.15 V vs. Ag/AgCl) was 510 mV more positive than the reaction without silver ($E_{cathode}$ = −1.66 V vs. Ag/AgCl). This shift in potential (effectively a lower overpotential) could prevent the over-reduction of the catalyst which we believe to be responsible for the passivation of the electrode. To test this hypothesis (Figure 4C-II), the reaction was run with doubled catalyst loading [$NiCl_2$•$6H_2O$ (20 mol%), 2,2’-bpy (20 mol%] which resulted in a modest 13% increase in yield in the absence of the silver salt. Next, the cross-coupling reaction was run at a constant potential of −1.15 V vs. Ag/AgCl with standard catalyst loading without a silver salt. These conditions resulted in a 10% increase in the yield of **39**. Furthermore, a reaction conducted with intermittent potential excursions to +1.5 V (70 s at +1.5 V vs. Ag/AgCl for every 11.5 mins of −6 mA), resulted in an 11% increase in the yield of **39**, consistent with the results of the RDE experiments and further providing evidence for catalyst over-reduction, and electrode passivation, at more forcing potentials—a deleterious process partially obviated by the silver layer.

A comparison of the Levich (I vs $\omega^{-1/2}$) analysis (Figure 4C-III) of the catalyst and the RAE **7** showed that diffusion of $NiCl_2$(bpy) was not significantly impacted by the silver nanoparticle layer (the calculated diffusion coefficient decreased by a factor of 2).(45) However, **7** showed a significant change in its diffusion behavior on the silver nanoparticle functionalized RDE. While at slow rates of rotation the currents at the bare and Ag modified electrodes were comparable, at faster rates of rotations there was a clear

divergence. Moreover, upon extrapolation to zero rotation, the intercept is clearly non-zero, suggesting possible adsorptive effects. To investigate if the reduction is occurring at the Ag nanoparticles or at the surface of the carbon electrode, the CVs of the RAE and the Ni catalyst at a Ag electrode and a glassy carbon electrode were compared to that of a Ag nanoparticle modified glassy carbon electrode (Figure S93). The Ag modified electrode exhibited the same features as the glassy carbon electrode, while not those of the Ag electrode, suggesting that the majority of the reductive events likely occur at the glassy carbon surface and require the redox active species to diffuse through the Ag NP film to be reduced. Taken collectively with the results of reaction progress over time (See SM, Figure S19-20), these results suggest that a decrease in direct reduction of RAE at the cathode is likely responsible, at least in part, for the improved reaction yield.

Investigations of the vinyl iodides **5** and **40** revealed that while direct reduction does not occur, significant differences in behavior exist between these two model vinyl iodides when $NiCl_2$(bpy) and RAE are present (Figure 4C-IV). When RDE voltammetry was conducted using $NiCl_2$(bpy) and **40**, a catalytic current response was observed at the Ni(0)/Ni(II) redox couple (resulting from the oxidative addition of the vinyl iodide) consistent with ECcat kinetics and the previously mentioned electrode passivation. Furthermore, in the presence of RAE **7**, this passivation behavior disappeared when using the methyl ester vinyl iodide **40**. Interestingly, use of halo-acid **5** in these measurements generated a catalytic current without significant electrode passivation even in the absence of RAE. Surprisingly, after addition of RAE **7** to halo-acid **5** and $NiCl_2$(bpy), the second reduction wave was still observed at −1.48 V vs Ag/AgCl potential. We propose this wave is the electrochemical reduction of a nickel (II/III) alkenyl to a nickel (I) alkenyl intermediate. (46,47) This profound difference in behavior when using halo-acid **5** instead of methyl ester **40** has significant implications on the detrimental behavior of carboxylic acids on reaction yield in the absence of $AgNO_3$. Recent evidence has emerged suggesting the deactivation of nickel (I) intermediates through dimerization or aggregation. (48) One can also imagine how this reduced species could accelerate the consumption of RAE in the homogeneous environment. (49). Comparing the onset of these two reduction waves to the cathode potential of the reaction without $AgNO_3$ ($E_{cathode}$ = −1.66 V vs. Ag/AgCl) and with $AgNO_3$ ($E_{cathode}$ = −1.15 V vs. Ag/AgCl) is particularly informative. This finding implied that the Ag-NP layer decreases overpotential to the point immediately prior to the second reduction wave whereas with the use of bare glassy carbon electrodes, more reducing potentials beyond the second wave under standard reaction conditions (constant current) are applied.

In summary, it appears that the silver-nanoparticle layer on the electrode has several effects on the reaction components. First, the silver-NP layer lowers the overpotential preventing catalyst over-reduction and electrode passivation. Second, the lower overpotential also inhibits the formation of Ni(I)-alkenyl intermediates which appear to form even in the presence of RAEs when using vinyl iodides bearing carboxylic acids. Third, this layer slows mass transport and reduction of RAEs at the electrode surface likely from complications arising with adsorptive behavior, while diffusion of the catalyst is only minorly affected. Though no singular result explains the role of the silver-nanoparticle layer, we hypothesize that the overall benefit observed is likely the result of the findings discussed above working

together in concert. Further interdisciplinary studies between synthetic, electroanalytical, and materials specialists will likely provide deeper insights into this unique discovery.

Outlook.

This study of terpene synthesis has provided an efficient platform for the modular construction of polyunsaturated molecules with precise geometrical control.(50) Its implementation required methodological advancement thereby revealing a relationship between productive catalysis and materials science. Electrochemistry offers chemists enabling opportunities through variables that are uniquely available to it. Electrode modification offers new possibilities for synthetic chemists to optimize difficult reactions —analytical chemists and physical chemists have long embraced this concept to overcome their own chemical challenges. The potential of these unique parameters to enable useful chemical reactivity is an attractive area for further study.

Supplementary Material

Refer to Web version on PubMed Central for supplementary material.

Acknowledgments

We thank D.-H. H. and L. P. for assistance with NMR spectroscopy; J. Chen, B Sanchez, and E. Sturgell for (Scripps Automated Synthesis Facility) for assistance with HPLC, HRMS, and LCMS; A. Rheingold, M. Gembicky, and E. Samolova, (University of California, San Diego) for assistance with x-ray crystallography; we are grateful to University of Utah shared facilities of the Micron Technology Foundation Inc.; We thank J. Vantourout, Kawamata, Y., S. Gnaim., Y.Y. See, J. Edwards, K. McClymont, C. Bi and B. Smith for insightful discussions; K. X. Rodriguez, J. Gu, A. L. Rerick, and C. R. Pitts, for their use of this chemistry in other systems, and K. Eberle, G. Laudadio, A. Garrido-Castro, and M. Condakes for assistance in the preparation of the manuscript.

Funding:

Financial support for this work was provided by the NIH (MIRA GM-118176), NSF Center for Synthetic Organic Electrochemistry (CHE-2002158) and the Microscopy Suite sponsored by the College of Engineering, Health Sciences Center, Office of the Vice President for Research, the Utah Science Technology and Research (USTAR) initiative of the State of Utah and, in part, by the MRSEC Program of the NSF under Award No. DMR-1121252. S.J.H. thanks the Fletcher-Jones Foundation for fellowship funding. M.D.P. thanks Richard and Nicola Lerner for the Endowed Fellowship.

References

1. Nicolaou KC, Sorenson EJ, Classics in Total Synthesis: Targets, Strategies, Methods. (1997), pp. xxii–798.
2. Cox-Georgian D, Ramadoss N, Dona C, Basu C, Therapeutic and Medicinal Uses of Terpenes. Medicinal Plants, 333–359 (2019).
3. Jansen DJ, Shenvi RA, Synthesis of medicinally relevant terpenes: reducing the cost and time of drug discovery. Future Med. Chem 6, 1127–1148 (2014). [PubMed: 25078134]
4. Serra S, in Studies in Natural Products Chemistry, Atta ur R, Ed. (Elsevier, 2015), vol. 46, pp. 201–226.
5. Johnson WS, Gravestock MB, McCarry BE, Acetylenic bond participation in biogenetic-like olefinic cyclizations. II. Synthesis of dl-progesterone. J. Am. Chem. Soc 93, 4332–4334 (1971). [PubMed: 5131151]
6. Yoder RA, Johnston JN, A Case Study in Biomimetic Total Synthesis: Polyolefin Carbocyclizations to Terpenes and Steroids. Chem. Rev 105, 4730–4756 (2005). [PubMed: 16351060]

7. Ungarean CN, Southgate EH, Sarlah D, Enantioselective polyene cyclizations. Org. Biomol. Chem 14, 5454–5467 (2016). [PubMed: 27143099]
8. Thirsk C, Whiting A, Polyene natural products. J. Chen. Soc. Perkin Trans I, 999–1023 (2002).
9. Negishi E.-i., Wang G, Rao H, Xu Z, Alkyne Elementometalation–Pd-Catalyzed Cross-Coupling. Toward Synthesis of All Conceivable Types of Acyclic Alkenes in High Yields, Efficiently, Selectively, Economically, and Safely: "Green" Way. J. Org. Chem 75, 3151–3182 (2010). [PubMed: 20465291]
10. Li J, Grillo AS, Burke MD, From Synthesis to Function via Iterative Assembly of N-Methyliminodiacetic Acid Boronate Building Blocks. Acc. Chem. Res 48, 2297–2307 (2015). [PubMed: 26200460]
11. Dewick PM, The mevalonate and methylerythritol phosphate pathways: Terpenoids and steroids. Medicinal Natural Products; A biosynthetic approach 2, 167–289 (2002).
12. Smith JM, Harwood SJ, Baran PS, Radical Retrosynthesis. Acc. Chem. Res 51, 1807–1817 (2018). [PubMed: 30070821]
13. Peters DS, Pitts CR, McClymont KS, Stratton TP, Bi C, Baran PS, Ideality in Context: Motivations for Total Synthesis. Acc. Chem. Res 54, 605–617 (2021). [PubMed: 33476518]
14. Edwards JT, Merchant RR, McClymont KS, Knouse KW, Qin T, Malins LR, Vokits B, Shaw SA, Bao D-H, Wei F-L, Zhou T, Eastgate MD, Baran PS, Decarboxylative alkenylation. Nature 545, 213–218 (2017). [PubMed: 28424520]
15. Cannes C, Condon S, Durandetti M, Périchon J, Nédélec JY, Nickel-Catalyzed Electrochemical Couplings of Vinyl Halides: Synthetic and Stereochemical Aspects. J. Org. Chem 65, 4575–4583 (2000). [PubMed: 10959862]
16. Novaes LFT, Liu J, Shen Y, Lu L, Meinhardt JM, Lin S, Electrocatalysis as an enabling technology for organic synthesis. Chem. Soc. Rev 50, 7941–8002 (2021). [PubMed: 34060564]
17. Wirtanen T, Prenzel T, Tessonnier J-P, Waldvogel SR, Cathodic Corrosion of Metal Electrodes—How to Prevent It in Electroorganic Synthesis. Chem. Rev 121, 10241–10270 (2021). [PubMed: 34228450]
18. Campelo JM, Luna D, Luque R, Marinas JM, Romero AA, Sustainable Preparation of Supported Metal Nanoparticles and Their Applications in Catalysis. ChemSusChem 2, 18–45 (2009). [PubMed: 19142903]
19. Huihui KMM, Caputo JA, Melchor Z, Olivares AM, Spiewak AM, Johnson KA, DiBenedetto TA, Kim S, Ackerman LKG, Weix DJ, Decarboxylative Cross-Electrophile Coupling of N-Hydroxyphthalimide Esters with Aryl Iodides. J. Am. Chem. Soc 138, 5016–5019 (2016). [PubMed: 27029833]
20. Koyanagi T, Herath A, Chong A, Ratnikov M, Valiere A, Chang J, Molteni V, Loren J, One-Pot Electrochemical Nickel-Catalyzed Decarboxylative Sp2–Sp3 Cross-Coupling. Org. Lett 21, 816–820 (2019). [PubMed: 30673257]
21. Li H, Breen CP, Seo H, Jamison TF, Fang Y-Q, Bio MM, Ni-Catalyzed Electrochemical Decarboxylative C–C Couplings in Batch and Continuous Flow. Org. Lett 20, 1338–1341 (2018). [PubMed: 29431449]
22. Perkins RJ, Pedro DJ, Hansen EC, Electrochemical Nickel Catalysis for Sp2-Sp3 Cross-Electrophile Coupling Reactions of Unactivated Alkyl Halides. Org. Lett 19, 3755–3758 (2017). [PubMed: 28704055]
23. Slegeris R, Dudley GB, Alternative synthetic approaches to rac-progesterone by way of the classic Johnson cationic polycyclization strategy. Tetrahedron 72, 3666–3672 (2016).
24. Camelio AM, Johnson TC, Siegel D, Total Synthesis of Celastrol, Development of a Platform to Access Celastroid Natural Products. J. Am. Chem. Soc 137, 11864–11867 (2015). [PubMed: 26331410]
25. Snider BB, Kiselgof JY, Foxman BM, Total Syntheses of (±)-Isosteviol and (±)-Beyer-15-ene-3β,19-diol by Manganese(III)-Based Oxidative Quadruple Free-Radical Cyclization. J. Org. Chem 63, 7945–7952 (1998).
26. Walker RP, Faulkner DJ, Diterpenes from the sponge Dysidea amblia. J. Org. Chem 46, 1098–1102 (1981).

27. Thompson JE, Walker RP, Faulkner DJ, Screening and bioassays for biologically-active substances from forty marine sponge species from San Diego, California, USA. Mar. Biol 88, 11–21 (1985).
28. Serra S, Lissoni V, First Enantioselective Synthesis of Marine Diterpene Ambliol-A. Eur. J. Org. Chem 2015, 2226–2234 (2015).
29. Scheffrahn RH, Gaston LK, Sims JJ, Rust MK, Identification of the defensive secretion from soldiers of the North American termite,Amitermes wheeleri (Desneux) (Isoptera: Termitidae). J. Chem. Ecol 9, 1293–1305 (1983). [PubMed: 24407859]
30. Roelofs WL, Gieselmann MJ, CardÉ AM, Tashiro H, Moreno DS, Henrick CA, Anderson RJ, Sex pheromone of the California red scale, Aonidiella aurantii. Nature 267, 698–699 (1977). [PubMed: 559950]
31. Weix DJ, Methods and Mechanisms for Cross-Electrophile Coupling of Csp2 Halides with Alkyl Electrophiles. Acc. Chem. Res 48, 1767–1775 (2015). [PubMed: 26011466]
32. Brito C, Jordão VL, Pierce GJ, Ambergris as an overlooked historical marine resource: its biology and role as a global economic commodity. J. Mar. Biol. Assoc. U. K 96, 585–596 (2016).
33. Barrero AF, Altarejos J, Alvarez-Manzaneda EJ, Ramos JM, Salido S, Synthesis of (±)-Ambrox from (E)-Nerolidol and β-Ionone via Allylic Alcohol [2,3] Sigmatropic Rearrangement. J. Org. Chem 61, 2215–2218 (1996).
34. Schubert V, Dietrich A, Ulrich T, Mosandl A, The Stereoisomers of Nerolidol: Separation, Analysis and Olfactoric Properties. Zeitschrift für Naturforschung C 47, 304–307 (1992).
35. Ben Salha G, Abderrabba M, Labidi J, A status review of terpenes and their separation methods. Rev. Chem. Eng 37, 433–447 (2021).
36. Chan W-K, Tan LT, Chan K-G, Lee L-H, Goh B-H, Nerolidol: A Sesquiterpene Alcohol with Multi-Faceted Pharmacological and Biological Activities. Molecules 21, 529 (2016).
37. McGinty D, Letizia CS, Api AM, Addendum to Fragrance material review on Nerolidol (isomer unspecified). Food and Chemical Toxicology 48, S43–S45 (2010). [PubMed: 20141875]
38. Dong X-Y, Gao Z-W, Yang K-F, Zhang W-Q, Xu L-W, Nanosilver as a new generation of silver catalysts in organic transformations for efficient synthesis of fine chemicals. Catalysis Science & Technology 5, 2554–2574 (2015).
39. Chillawar RR, Tadi KK, Motghare RV, Voltammetric techniques at chemically modified electrodes. J. Anal. Chem 70, 399–418 (2015).
40. Zen J-M, Senthil Kumar A, Tsai D-M, Recent Updates of Chemically Modified Electrodes in Analytical Chemistry. Electroanalysis 15, 1073–1087 (2003).
41. Nutting JE, Gerken JB, Stamoulis AG, Bruns DL, Stahl SS, “How Should I Think about Voltage? What Is Overpotential?”: Establishing an Organic Chemistry Intuition for Electrochemistry. J. Org. Chem, (2021).
42. Luo X, Morrin A, Killard AJ, Smyth MR, Application of Nanoparticles in Electrochemical Sensors and Biosensors. Electroanalysis 18, 319–326 (2006).
43. Welch CM, Banks CE, Simm AO, Compton RG, Silver nanoparticle assemblies supported on glassy-carbon electrodes for the electro-analytical detection of hydrogen peroxide. Analytical and Bioanalytical Chemistry 382, 12–21 (2005). [PubMed: 15900446]
44. Fox CM, Breslin CB, Electrochemical formation of silver nanoparticles and their applications in the reduction and detection of nitrates at neutral pH. J. Appl. Electrochem 50, 125–138 (2020).
45. Karuppiah C, Muthupandi K, Chen S-M, Ali MA, Palanisamy S, Rajan A, Prakash P, Al-Hemaid FMA, Lou B-S, Green synthesized silver nanoparticles decorated on reduced graphene oxide for enhanced electrochemical sensing of nitrobenzene in waste water samples. RSC Adv. 5, 31139–31146 (2015).
46. Isse AA, Gottardello S, Maccato C, Gennaro A, Silver nanoparticles deposited on glassy carbon. Electrocatalytic activity for reduction of benzyl chloride. Electrochem. Commun 8, 1707–1712 (2006).
47. Ren X, Meng X, Chen D, Tang F, Jiao J, Using silver nanoparticle to enhance current response of biosensor. Biosens. Bioelectron 21, 433–437 (2005). [PubMed: 16076432]
48. Manohar AB, Bhalchandra MB, Silver Nanoparticles: Synthesis, Characterization and their Application as a Sustainable Catalyst for Organic Transformations. Current Organic Chemistry 19, 708–727 (2015).

49. Compton RG, Laing ME, Mason D, Northing RJ, Unwin PR, Rowlinson JS, Rotating disc electrodes: the theory of chronoamperometry and its use in mechanistic investigations. Proc. Math. Phys. Eng. Sci 418, 113–154 (1988).
50. Gu J, Rodriguez KX, Kanda Y, Yang S, Oceipa M, Wilke H, Abrishami AV, Jørgensen L, Skak-Nielsen T, Chen JS, Baran PS, Convergent Total Synthesis of (+)-Calcipotriol: A Scalable Modular Approach to Vitamin D Analogs. ChemRxiv. Cambridge: Cambridge Open Engage, doi:10.26434/chemrxiv-2021-kn6tl (2021)
51. Royzen M, Yap GPA, Fox JM, A Photochemical Synthesis of Functionalized trans-Cyclooctenes Driven by Metal Complexation. J. Am. Chem. Soc 130, 3760–3761 (2008). [PubMed: 18321114]
52. Edwards JT, Merchant RR, McClymont KS, Knouse KW, Qin T, Malins LR, Vokits B, Shaw SA, Bao D-H, Wei F-L, Zhou T, Eastgate MD, Baran PS, Decarboxylative alkenylation. Nature 545, 213–218 (2017). [PubMed: 28424520]
53. Hötling S, Haberlag B, Tamm M, Collatz J, Mack P, Steidle JLM, Vences M, Schulz S, Identification and Synthesis of Macrolide Pheromones of the Grain Beetle Oryzaephilus Surinamensis and the Frog Spinomantis Aglavei. Chem. Eur. J 20, 3183–3191 (2014). [PubMed: 24523150]
54. Jiang X, Zhang J, Ma S, Iron Catalysis for Room-Temperature Aerobic Oxidation of Alcohols to Carboxylic Acids. J. Am. Chem. Soc 138, 8344–8347 (2016). [PubMed: 27304226]
55. Fürstner A, Flügge S, Larionov O, Takahashi Y, Kubota T, Kobayashi J. i., Total Synthesis and Biological Evaluation of Amphidinolide V and Analogues. Chem. Eur. J 15, 4011–4029 (2009). [PubMed: 19241434]
56. Van Horn DE, Negishi E, Selective carbon-carbon bond formation via transition metal catalysts. 8. Controlled carbometalation. Reaction of acetylenes with organoalane-zirconocene dichloride complexes as a route to stereo- and regio-defined trisubstituted olefins. J. Am. Chem. Soc 100, 2252–2254 (1978).
57. Liu Q, Hu P, He Y, Asymmetric Total Synthesis of Nannocystin A. J. Org. Chem 82, 9217–9222 (2017). [PubMed: 28787157]
58. Schrof R, Altmann K-H, Studies toward the Total Synthesis of the Marine Macrolide Salarin C. Org. Lett 20, 7679–7683 (2018). [PubMed: 30474982]
59. Slegeris R, Dudley GB, Alternative synthetic approaches to rac-progesterone by way of the classic Johnson cationic polycyclization strategy. Tetrahedron 72, 3666–3672 (2016).
60. Davies JA, Bull FM, Walker PD, Weir ANM, Lavigne R, Masschelein J, Simpson TJ, Race PR, Crump MP, Willis CL, Total Synthesis of Kalimantacin A. Org. Lett 22, 6349–6353 (2020). [PubMed: 32806153]
61. Richter A, Hedberg C, Waldmann H, Enantioselective Synthesis of the C10–C20 Fragment of Fusicoccin A. J. Org. Chem 76, 6694–6702 (2011). [PubMed: 21755994]
62. Malhotra R, Rarhi C, Diveshkumar KV, Barik R, D'cunha R, Dhar P, Kundu M, Chattopadhyay S, Roy S, Basu S, Pradeepkumar PI, Hajra S, Dihydrochelerythrine and its derivatives: Synthesis and their application as potential G-quadruplex DNA stabilizing agents. Bioorg. Med. Chem 24, 2887–2896 (2016). [PubMed: 27234888]
63. Miwa K, Aoyama T, Shiori T, A New Synthesis of 5-Trimethylsilyl-2,3-dihydrofurans from β-Trimethylsiloxyketones Utilizing Trimethylsilyldiazomethan. Synlett 1994, 461–462 (1994).
64. Camelio AM, Johnson TC, Siegel D, Total Synthesis of Celastrol, Development of a Platform to Access Celastroid Natural Products. J. Am. Chem. Soc 137, 11864–11867 (2015). [PubMed: 26331410]
65. Karjalainen OK, Passiniemi M, Koskinen AMP, Short and Straightforward Synthesis of (−)-1-Deoxygalactonojirimycin. Org. Lett 12, 1145–1147 (2010). [PubMed: 20170191]
66. Layton ME, Morales CA, Shair MD, Biomimetic Synthesis of (−)-Longithorone A. J. Am. Chem. Soc 124, 773–775 (2002). [PubMed: 11817951]
67. House HO, Chu C-Y, Wilkins JM, Umen MJ, Chemistry of carbanions. XXVII. Convenient precursor for the generation of lithium organocuprates. J. Org. Chem 40, 1460–1469 (1975).
68. Snider BB, Kiselgof JY, Foxman BM, Total Syntheses of (±)-Isosteviol and (±)-Beyer-15-ene-3β,19-diol by Manganese(III)-Based Oxidative Quadruple Free-Radical Cyclization. J. Org. Chem 63, 7945–7952 (1998).

69. Fang H-J, Shou X-A, Liu Q, Gan C-C, Duan H-Q, Qin N, Synthesis and anti-metastatic effects of novel chiral ionone alkaloid derivatives. Eur. J. Med. Chem 101, 245–253 (2015). [PubMed: 26142489]
70. Wang Z-X, Tu Y, Frohn M, Zhang J-R, Shi Y, An Efficient Catalytic Asymmetric Epoxidation Method. J. Am. Chem. Soc 119, 11224–11235 (1997).
71. Serra S, Lissoni V, First Enantioselective Synthesis of Marine Diterpene Ambliol-A. European Journal of Organic Chemistry 2015, 2226–2234 (2015).
72. Walker RP, Faulkner DJ, Diterpenes from the sponge Dysidea amblia. J. Org. Chem 46, 1098–1102 (1981).
73. Miller KK, Zhang P, Nishizawa-Brennen Y, Frost JW, Synthesis of Biobased Terephthalic Acid from Cycloaddition of Isoprene with Acrylic Acid. ACS Sustain. Chem. Eng 2, 2053–2056 (2014).
74. Cusack NJ, Reese CB, Risius AC, Roozepeikar B, 2,4,6-Tri-isopropylbenzenesulphonyl hydrazide: A convenient source of di-imide. Tetrahedron 32, 2157–2162 (1976).
75. Mikusek J, Nugent J, Lan P, Banwell MG, Chemical Synthesis Study Establishes the Correct Structure of the Potent Anti-Inflammatory Agent Myrsinoic Acid F. J. Nat. Prod 82, 96–100 (2019). [PubMed: 30589258]
76. Negishi E.-i., King AO, Tour JM, Conversion of Methyl Ketones into Terminal Alkynes: (E)-buten-3-ynyl-2,6,6-trimethyl-1-cyclohexene. Org. Synth 64, 44–49 (1986).
77. Salvaggio F, Hodgkinson JT, Carro L, Geddis SM, Galloway WRJD, Welch M, Spring DR, The Synthesis of Quinolone Natural Products from Pseudonocardia sp. Eur. J. Org. Chem 2016, 434–437 (2016).
78. Wang J-X, Total Synthesis of plakortones A, B, and E; Synthesis of cyclic peroxides by ring closing metathesis and synthesis and stereochemistry of (+)-Zerumin B & beyond., Université Laval., (2007).
79. Delay F, Ohloff G, Syntheses and Absolute Configuration of (E)- and (Z)-α-Bisabolenes. Helv. Chim. Acta 62, 369–377 (1979).
80. Ito F, Ohbatake Y, Aoyama S, Ikeda T, Arima S, Yamada Y, Ikeda H, Nagamitsu T, Total Synthesis of (+)-Clavulatriene A. Synthesis 47, 1348–1355 (2015).
81. Scheffrahn RH, Gaston LK, Sims JJ, Rust MK, Identification of the defensive secretion from soldiers of the North American termite,Amitermes wheeleri (Desneux) (Isoptera: Termitidae). J. Chem. Ecol 9, 1293–1305 (1983). [PubMed: 24407859]
82. Cook C, Guinchard X, Liron F, Roulland E, Total Synthesis of (−)-Exiguolide. Org. Lett 12, 744–747 (2010). [PubMed: 20078080]
83. Raghavan S, Sudheer Babu V, Total Synthesis of (+)-(2′S,3′R)-Zoapatanol Exploiting the B-Alkyl Suzuki Reaction and the Nucleophilic Potential of the Sulfinyl Group. Chem. Eur. J 17, 8487–8494 (2011). [PubMed: 21671292]
84. Ma S, Negishi E.-i., Anti-Carbometalation of Homopropargyl Alcohols and Their Higher Homologues via Non-Chelation-Controlled Syn-Carbometalation and Chelation-Controlled Isomerization. J. Org. Chem 62, 784–785 (1997).
85. Wang B, Lu C, Zhang S-Y, He G, Nack WA, Chen G, Palladium-Catalyzed Stereoretentive Olefination of Unactivated C(sp3)—H Bonds with Vinyl Iodides at Room Temperature: Synthesis of β-Vinyl α-Amino Acids. Org. Lett 16, 6260–6263 (2014). [PubMed: 25412205]
86. Cox LR, DeBoos GA, Fullbrook JJ, Percy JM, Spencer NS, Tolley M, Catalytic Asymmetric Synthesis of a 1-Deoxy-1,1-difluoro-d-xylulose. Org. Lett 5, 337–339 (2003). [PubMed: 12556186]
87. Madden KS, Jokhoo HRE, Conradi FD, Knowles JP, Mullineaux CW, Whiting A, Using Nature's polyenes as templates: studies of synthetic xanthomonadin analogues and realising their potential as antioxidants. Org. Biomol. Chem 17, 3752–3759 (2019). [PubMed: 30840015]
88. Hesse MJ, Butts CP, Willis CL, Aggarwal VK, Diastereodivergent Synthesis of Trisubstituted Alkenes through Protodeboronation of Allylic Boronic Esters: Application to the Synthesis of the Californian Red Scale Beetle Pheromone. Angew. Chem. Int. Ed 51, 12444–12448 (2012).
89. Roelofs W, Gieselmann M, Cardé A, Tashiro H, Moreno DS, Henrick CA, Anderson RJ, Identification of the California red scale sex pheromone. J. Chem. Ecol 4, 211–224 (1978).

90. Kobayashi S, Ando A, Kuroda H, Ejima S, Masuyama A, Ryu I, Rapid access to 6-bromo-5,7-dihydroxyphthalide 5-methyl ether by a CuBr2-mediated multi-step reaction: concise total syntheses of hericenone J and 5′-deoxohericenone C (hericene A). Tetrahedron 67, 9087–9092 (2011).
91. Godeau J, Fontaine-Vive F, Antoniotti S, Duñach E, Experimental and Theoretical Studies on the Bismuth-Triflate-Catalysed Cycloisomerisation of 1,6,10-Trienes and Aryl Polyenes. Chem. Eur. J 18, 16815–16822 (2012). [PubMed: 23143886]
92. Cermak DM, Wiemer DF, Lewis K, Hohl RJ, 2-(Acyloxy)ethylphosphonate analogues of prenyl pyrophosphates: synthesis and biological characterization. Bioorg. Med. Chem 8, 2729–2737 (2000). [PubMed: 11131164]
93. Kocieński PJ, Pritchard M, Wadman SN, Whitby RJ, Yeates CL, A stereoselective synthesis of trisubstituted alkenes. Part 1. Nickel-catalysed coupling of Grignard reagents with 5-alkyl-2,3-dihydrofurans. J. Chen. Soc. Perkin Trans I, 3419–3429 (1992).
94. Ilardi EA, Stivala CE, Zakarian A, Hexafluoroisopropanol as a Unique Solvent for Stereoselective Iododesilylation of Vinylsilanes. Org. Lett 10, 1727–1730 (2008). [PubMed: 18386904]
95. Radosevich AT, Chan VS, Shih H-W, Toste FD, Synthesis of (−)-Octalactin A by a Strategic Vanadium-Catalyzed Oxidative Kinetic Resolution. Angew. Chem. Int. Ed 47, 3755–3758 (2008).
96. Kocienski P, Wadman S, Cooper K, A highly stereoselective and iterative approach to isoprenoid chains: synthesis of homogeraniol, homofarnesol, and homogeranylgeraniol. J. Org. Chem 54, 1215–1217 (1989).
97. Svatoš A, Urbanová K, Valterová I, The First Synthesis of Geranyllinalool Enantiomers. Collect. Czech. Chem. Commun 67, 83–90 (2002).
98. Cane DE, Ha H-J, McIlwaine DB, Pascoe KO, The synthesis of (3R)-nerolidol. Tetrahedron Lett. 31, 7553–7554 (1990).
99. Cochran BM, One-Pot Oxidative Cleavage of Olefins to Synthesize Carboxylic Acids by a Telescoped Ozonolysis–Oxidation Process. Synlett 27, 245–248 (2016).
100. Díaz L, Bujons J, Casas J, Llebaria A, Delgado A, Click Chemistry Approach to New N-Substituted Aminocyclitols as Potential Pharmacological Chaperones for Gaucher Disease. J. Med. Chem 53, 5248–5255 (2010). [PubMed: 20557054]
101. Schäckermann J-N, Lindel T, Synthesis and Photooxidation of the Trisubstituted Oxazole Fragment of the Marine Natural Product Salarin C. Org. Lett 19, 2306–2309 (2017). [PubMed: 28425712]
102. González-García J, Bonete P, Expósito E, Montiel V, Aldaz A, Torregrosa-Maciá R, Characterization of a carbon felt electrode: structural and physical properties. J. Mater. Chem 9, 419–426 (1999).
103. Kigoshi H, Ojika M, Shizuri Y, Niwa H, Yamada K, Isolation of (10R,11R)-(+)-squalene-10,11-epoxide from the red alga laurencia okamurai and its enantioselective synthesis. Tetrahedron 42, 3789–3792 (1986).
104. Schubert V, Dietrich A, Ulrich T, Mosandl A, The Stereoisomers of Nerolidol: Separation, Analysis and Olfactoric Properties. Zeitschrift für Naturforschung C 47, 304–307 (1992).
105. Cane DE, Iyengar R, Shiao M-S, Cyclonerodiol biosynthesis and the enzymic conversion of farnesyl to nerolidyl pyrophosphate. J. Am. Chem. Soc 103, 914–931 (1981).
106. del Castillo JB, Brooks CJW, Campbell MM, Caparrapidiol and caparrapitriol: Two new acyclic sesquiterpene alcohols. Tetrahedron Lett. 7, 3731–3736 (1966).
107. Clark RD, Heathcock CH, Reduction of .beta.-halo-.alpha.,.beta.-unsaturated ketones. J. Org. Chem 38, 3658–3658 (1973).
108. Klein A, Synthesis, Spectroscopic Properties, and Crystal Structure of 2,2′-Bipyridyldimesitylnickel(II). Zeitschrift für anorganische und allgemeine Chemie 627, 645–650 (2001).
109. Klein A, Kaiser A, Wielandt W, Belaj F, Wendel E, Bertagnolli H, Záliš S, Halide Ligands—More Than Just σ-Donors? A Structural and Spectroscopic Study of Homologous Organonickel Complexes. Inorg. Chem 47, 11324–11333 (2008). [PubMed: 18959362]

110. Zhang Z-X, Wang S, Li S-M, Shan S-L, Wang H, Lu J-X, Synthesis of Ag nanoparticles/ordered mesoporous carbon as a highly efficient catalyst for the electroreduction of benzyl bromide. RSC Adv. 10, 756–762 (2020). [PubMed: 35494476]

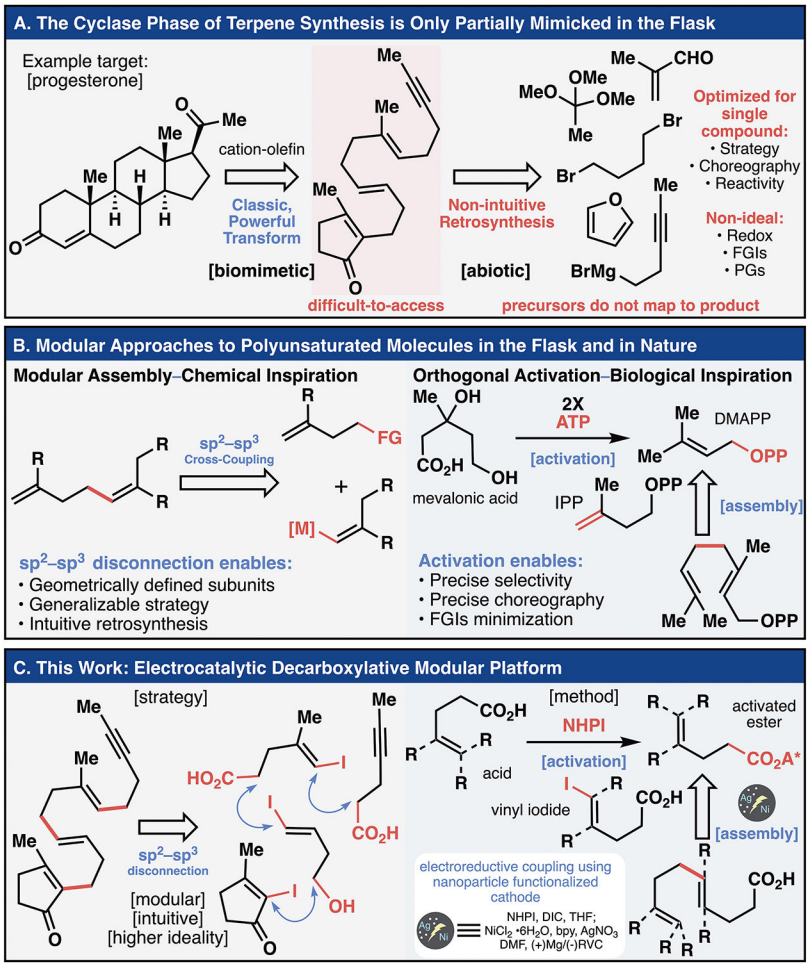

Fig. 1.

The synthesis of polyene cyclization precursors remains a challenge to chemists. Taking inspiration from chemical and natural precedent, this work developed a modular platform constructing sp^2–sp^3 bonds using an electrochemical reaction and functionalized electrodes. (A) Retrosynthetic analysis of Johnson's classic total synthesis of progesterone. (B) The advantages of a prototypical sp^2–sp^3 disconnection and the biosynthesis of geraniol pyrophosphate. Adenosine triphosphate (ATP) activation of an alcohol generates the reactive chemical feedstocks necessary for terpene synthesis. (C) Combining the advantages of the sp^2–sp^3 disconnection and the modular and selective activation characteristics of the biosynthesis required development of a mild reaction using nickel electrocatalysis and Ag-nanoparticle functionalized electrodes.

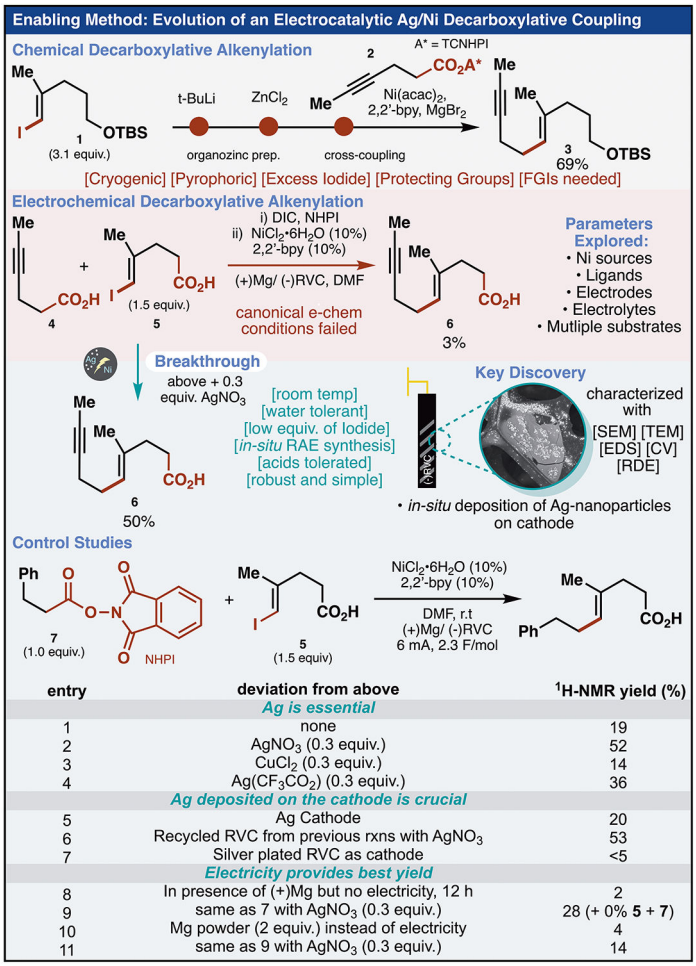

entry	deviation from above	^{1}H-NMR yield (%)
	Ag is essential	
1	none	19
2	$AgNO_3$ (0.3 equiv.)	52
3	$CuCl_2$ (0.3 equiv.)	14
4	$Ag(CF_3CO_2)$ (0.3 equiv.)	36
	Ag deposited on the cathode is crucial	
5	Ag Cathode	20
6	Recycled RVC from previous rxns with $AgNO_3$	53
7	Silver plated RVC as cathode	<5
	Electricity provides best yield	
8	In presence of (+)Mg but no electricity, 12 h	2
9	same as 7 with $AgNO_3$ (0.3 equiv.)	28 (+ 0% **5** + **7**)
10	Mg powder (2 equiv.) instead of electricity	4
11	same as 9 with $AgNO_3$ (0.3 equiv.)	14

Fig. 2.

The discovery and optimization of the electrocatalytic methodology is described. The published decarboxylative alkenylation is a prototypical example of literature methods to construct sp^2–sp^3 bonds requiring harsh reagents, cryogenic temperatures, protecting groups and functional group interconversions (FGIs). Initial electrochemical conditions were insufficient to accomplish the envisioned plan to cross-couple *in situ* activated acids and halo-acid modules. The addition of $AgNO_3$ (0.3 equiv.) to the reaction was a breakthrough. Control experimentation suggests that nanosilver on the cathode is responsible for the improved yield and that electrochemistry offers a unique advantage over other systems.

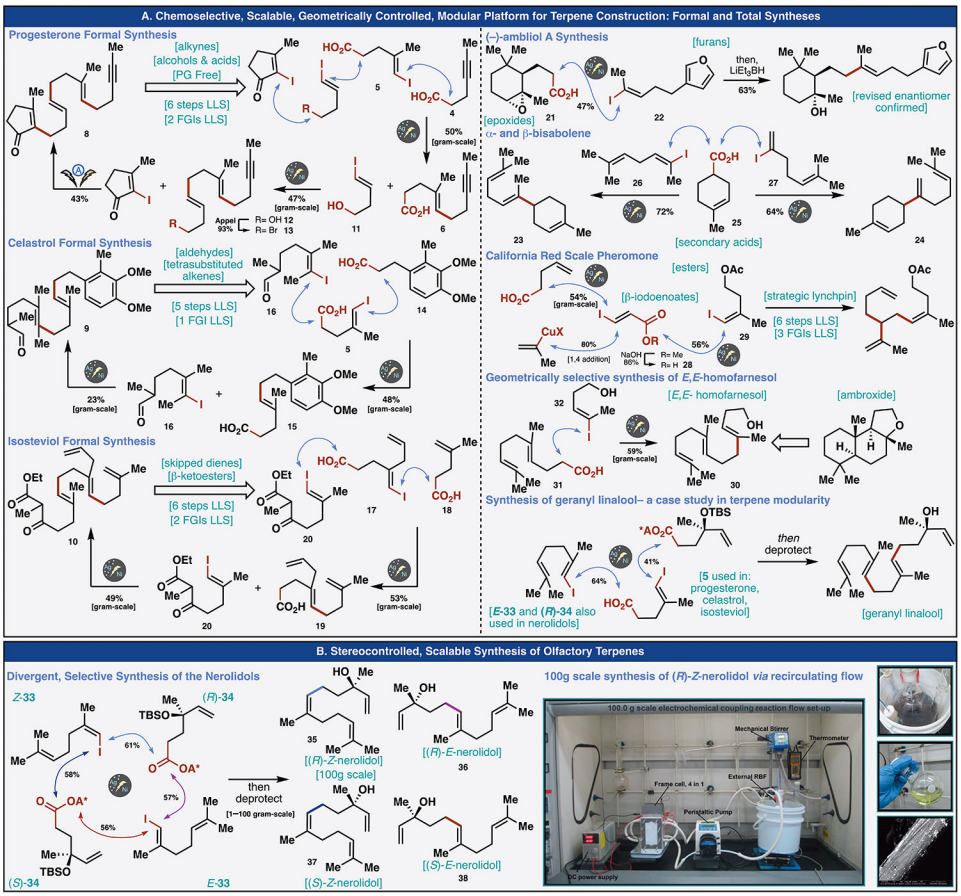

Fig. 3.

The utility and scalability of the developed electrocatalytic methodology is showcased through the formal or total synthesis of 13 natural products. (A) Three polyene cyclization precursors and five natural products are synthesized through iterative electrochemical cross-electrophile couplings showing a functional group tolerance inclusive of alkynes, alcohols, acids, esters, ketones, enones, aldehydes, ethers, epoxides, electron-rich heteroaromatics and skipped dienes. (B) A unified and scalable synthesis of the four nerolidol isomers is described. A recirculating flow system was used to conduct a 100g-scale electrochemical cross-coupling. The large image showcases the complete flow system consisting of a frame cell, power source, peristaltic pump, round bottom flask reservoir, and a mechanical stirrer. On right: (top) reaction reservoir, (middle) pure product after column chromatography, (bottom) SEM image of the Ag-nanoparticle embedded carbon felt cathode post-reaction.

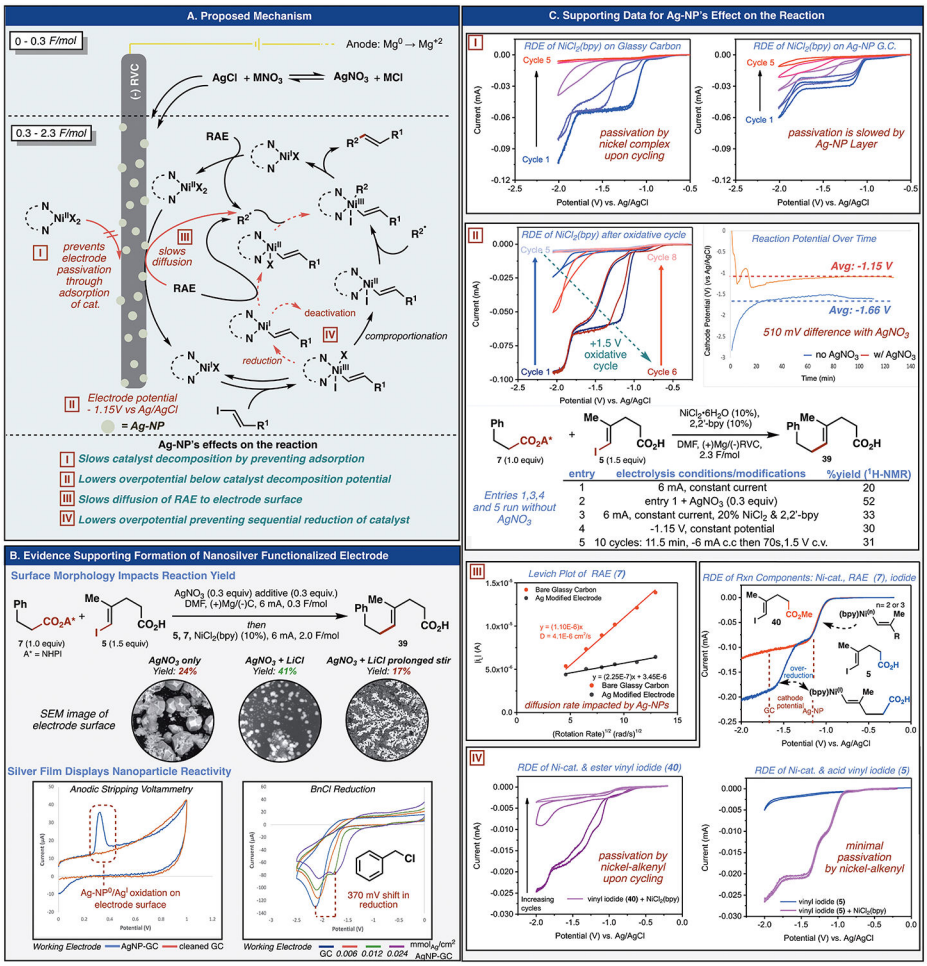

Fig. 4.

The presence of silver nanoparticles on the electrode surface is confirmed and the specific roles of the silver nanoparticle layer are posited. (A). A mechanism is proposed with Roman numerals indicating points of interaction with the Ag-nanoparticle layer. The silver layer slows catalyst decomposition (I), decreases overpotential so that the electrode potential falls below the decomposition potential (II), limits diffusion and mass transport of the RAE to the electrode surface (III), and adsorbs the acid-bearing vinyl iodide to the electrode surface (IV). (B) Control studies and S/TEM imaging identify that the reaction conditions produce Ag-nanoparticles on the electrode surface, a halide source is required, and photodecomposition of the silver-halide solution before electrolysis prevents nanoparticulate formation and diminishes the reaction yield. (C) Rotating disk electrode (RDE) voltammetry provides supporting evidence for the differences between the Ag-nanoparticle functionalized and unfunctionalized glassy carbon electrodes. [I] RDE voltammetric profiles (at 1600 rpm) of the Ni(bpy) catalyst at bare and Ag-NP modified glassy carbon electrodes. [II] Regeneration of activity, time evolution of cathode potential and product yields under various electrolysis conditions. [III] Levich plots (I vs $\omega^{-1/2}$) for $NiCl_2$(bpy) catalyst and RAE **7**. [IV] RDE voltammetric profiles of vinyl iodides **5** (right) and **40** (left) at bare glassy carbon electrodes exhibiting EC_{cat} kinetics (note the two reduction waves). RDE

voltammetric profile of reaction components (top) (1mM $NiCl_2$(bpy), 10 mM RAE **7**, 15 mM vinyl iodide (**40,** red trace; **5**, blue trace). Second reduction wave at present −1.48 V vs Ag/AgCl with **5,** but not with **40.**